Characteristics of penetration electric fields to the equatorial ionosphere during southward and northward IMF turnings

Ankush Bhaskar[1] and Geeta Vichare[1]

Received 1 February 2013; revised 27 May 2013; accepted 3 July 2013; published 31 July 2013.

[1] The signatures of abrupt turnings of the vertical component of the interplanetary magnetic field (IMF), Bz, can be seen at equatorial latitudes through the prompt transmission of high-latitude electric fields to the lower latitudes, called as prompt penetration electric field (PPE). The present work studies the signatures of PPE in daytime equatorial electrojet (EEJ) index derived in the Indian sector during 2001–2005. The signatures are observed in polar (PCN index) and equatorial (EEJ index) ionosphere almost instantaneously (< 1 min). The communication time of 12 ± 6 min is observed between bow shock nose and the equatorial ionosphere, and it is found to have inverse relationship with radial component of solar wind velocity during southward and northward Bz turnings which might indicate magnetosphere crossing time scale by solar wind. Ionospheric reconfiguration time during southward turnings shows inverse relationship with solar wind flow in contrast to northward turnings with "no relationship," indicating differences in underlying physical mechanisms during both turnings. We observe no local time dependence (within 06–18 h) in conductivity-corrected EEJ signatures associated with Bz turnings. Regression analysis between conductivity-corrected EEJ and interplanetary electric field shows higher efficiency during northward turnings. However, further analysis investigating the effect of actual orientation of Bz indicates that the magnitude of northward Bz does not have influence on the ionospheric signatures. It is noticed that the response signatures are mainly controlled by the magnitudes of southward Bz. Thus, the present study signifies the role of inner magnetospheric shielding electric field in addition to ceasing of convection during northward turnings.

Citation: Bhaskar, A., and G. Vichare (2013), Characteristics of penetration electric fields to the equatorial ionosphere during southward and northward IMF turnings, *J. Geophys. Res. Space Physics*, *118*, 4696–4709, doi:10.1002/jgra.50436.

1. Introduction

[2] It has been observed that the magnetic disturbances observed at the geomagnetic equator are usually correlated with simultaneous magnetic fluctuations at the high-latitude region, particularly polar region [*Onwumechilli and Ogbuehi*, 1962; *Nishida et al.*, 1966; *Nishida*, 1968; *Kikuchi et al.*, 1996, 2000]. The electric fields associated with these disturbances are termed as prompt penetration electric fields (PPE). These disturbances can be originated from different geophysical processes like geomagnetic sudden impulses, pulsations, geomagnetic storms, and substorms. The disturbance level at high-latitude and polar regions is generally governed by the interplanetary conditions, in which orientation of the interplanetary magnetic field (IMF) plays an important role. *Nishida* [1968] observed a good coherence of the vertical component of the IMF (Bz) with magnetic field variations at equatorial stations irrespective of its orientation and suggested the penetration of interplanetary electric field (IEF) as the origin for DP2 current system.

[3] The IEF gets mapped to the high latitude and transmits to the equator within the temporal resolution of tens of seconds. This almost instantaneous transmission is explained by using the zeroth-order transverse (TM_0) electromagnetic waves which propagate in the earth-ionosphere waveguide. It assumes that the Earth and ionosphere are infinitely conducting, and the insulating atmosphere between them generates waveguide [*Kikuchi et al.*, 1978; *Kikuchi and Araki*, 1979]. Due to the finite thickness of the earth-ionosphere waveguide, the transmitted electric field gets attenuated with decreasing latitude. But the effect of the PPE to the equator can be observed through the enhanced currents flowing in the *E* region. However, this has a limitation of being observed only during daytime, when sufficient conductivity exists in the *E* region.

[4] The working definition of PPE is the electric field of solar wind/magnetosphere origin observed equatorward (earthward) of the shielding layer [*Huang et al.*, 2006]. The definition accommodates the electric field changes resulting from the changes in the solar wind and IMF but excludes the overshielding electric field resulting from the Bz northward

[1]Indian Institute of Geomagnetism, Navi Mumbai, India.

Corresponding author: A. Bhaskar, Indian Institute of Geomagnetism, Plot 5, Sector 18, Navi Mumbai-410218, India. (ankushbhaskar@gmail.com)

2169-9380/13/10.1002/jgra.50436

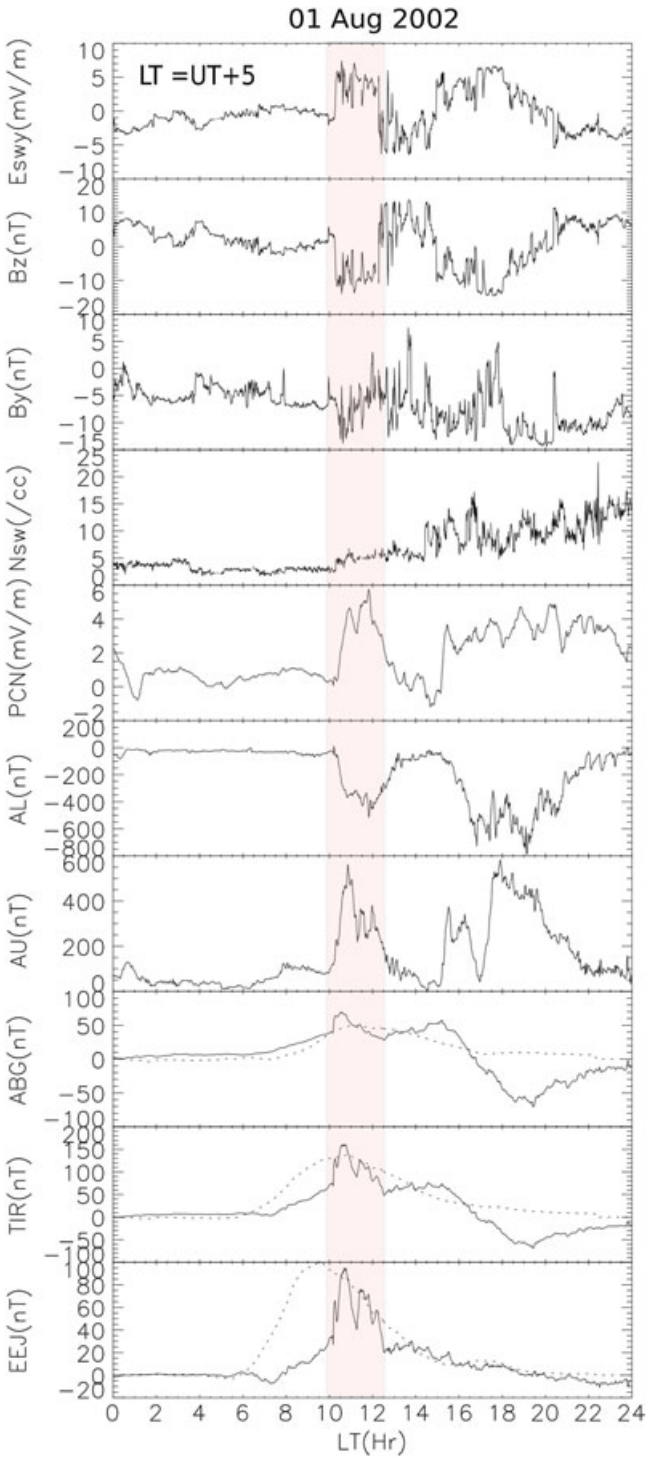

Figure 1. The geomagnetic and associated interplanetary parameters are shown in vertical stack plot on 01 August 2001. The LT is local time at 75° east longitude. The enhancement seen between 10:30 and 12:30 LT in EEJ is well correlated with variation in *H* component of geomagnetic field at ABG and TIR along with PCN, AL, AU, Eswy, and Bz, where as solar wind density shows absence of strong sharp variations. The dotted line represents the average of first five quiet days of August 2001.

turnings and the electric field affected due to the ionospheric disturbance dynamo [*Kelley et al.*, 1979; *Huang et al.*, 2006; *Wolf et al.*, 2007]. The disturbance dynamo is generated due to joule heating at high latitude and takes time to propagate to low latitude so signature is delayed by hours unlike PPE [*Blanc and Richmond*, 1980]. The characteristics of the penetration electric field during geomagnetic storms have been studied by researchers which includes penetration efficiency to equator, time scales, and longitudinal variation [*Kelley et al.*, 2003; *Manoj et al.*, 2008; *Tsuji et al.*, 2012]. *Tsuji et al.* [2012] observed magnetic local time (MLT) distribution of magnetic variation during the recovery phase reversed as compared to magnetic variation during the main phase in dayside middle latitude region. They ascribed the observed reversal to the overshielding electric field due to Region 2 field-aligned currents. *Manoj et al.* [2008] studied statistical characteristics of PPE as a function of time scale. They observed that coherence between the interplanetary electric field and the equatorial electric field peaks near 2 h period which might suggest the magnetosphere acting as capacitor. *Kelley et al.* [2003] found the ratio of the dawn-to-dusk component of IEF to that in the equatorial ionosphere to be 15:1, suggesting correspondence with the ratio of the size of the magnetopause to the length of the connection line between IMF and the Earth's magnetic field.

[5] *Huang et al.* [2007] reported an empirical value of 9.6% for the efficiency of penetration and showed that IEF can continuously penetrate to the low-latitude ionosphere without significant attenuation for many hours during the main phase of the geomagnetic storm, whereas *Fejer et al.* [2007] observed very strong and dynamic eastward and westward electrojet perturbations in equatorial electrojet currents which are indicative of undershielding and overshielding of PPE, when southward Bz, polar cap potential, and solar wind pressure had very large values and remain almost steady during the main phase of the geomagnetic storm of 7 November 2004. *Kikuchi et al.* [2010] reported the observations of eastward EEJ and westward EEJ during southward and northward IMF, respectively. Also, by studying SuperDARN convection maps they showed that the eastward equatorial electrojet (EEJ) is associated with the two-cell ionospheric convection vortex, whereas westward EEJ is accompanied by reverse flow vortices forming equatorward of the two-cell vortices.

[6] So though extensive work is carried out in understanding PPE, still many aspects of the phenomenon are controversial and yet to be resolved. PPE is a signature of magnetosphere-ionosphere (M-I) coupling which can be used to diagnose the physical mechanism underlying M-I coupling. Also, the quantification of the IEF transmission efficiency can probe the strength of the coupling and can throw some light on the possible mechanism of the coupling. It is important to note that mainly IMF orientation controls the transfer of solar wind energy to the magnetosphere. According to the model proposed by *Dungey* [1961], during southward Bz dayside reconnection occurs at low latitude, whereas for northward Bz it occurs at high latitude. During northward Bz conditions, some of the researchers observed reversed convection cells in high-latitude regions [*Iijima*, 1984; *Clauer and Friis-Christensen*, 1988; *Etemadi et al.*, 1988; *Khan and Cowley*, 1999], whereas some others reported weak convection rather than reversal of direction

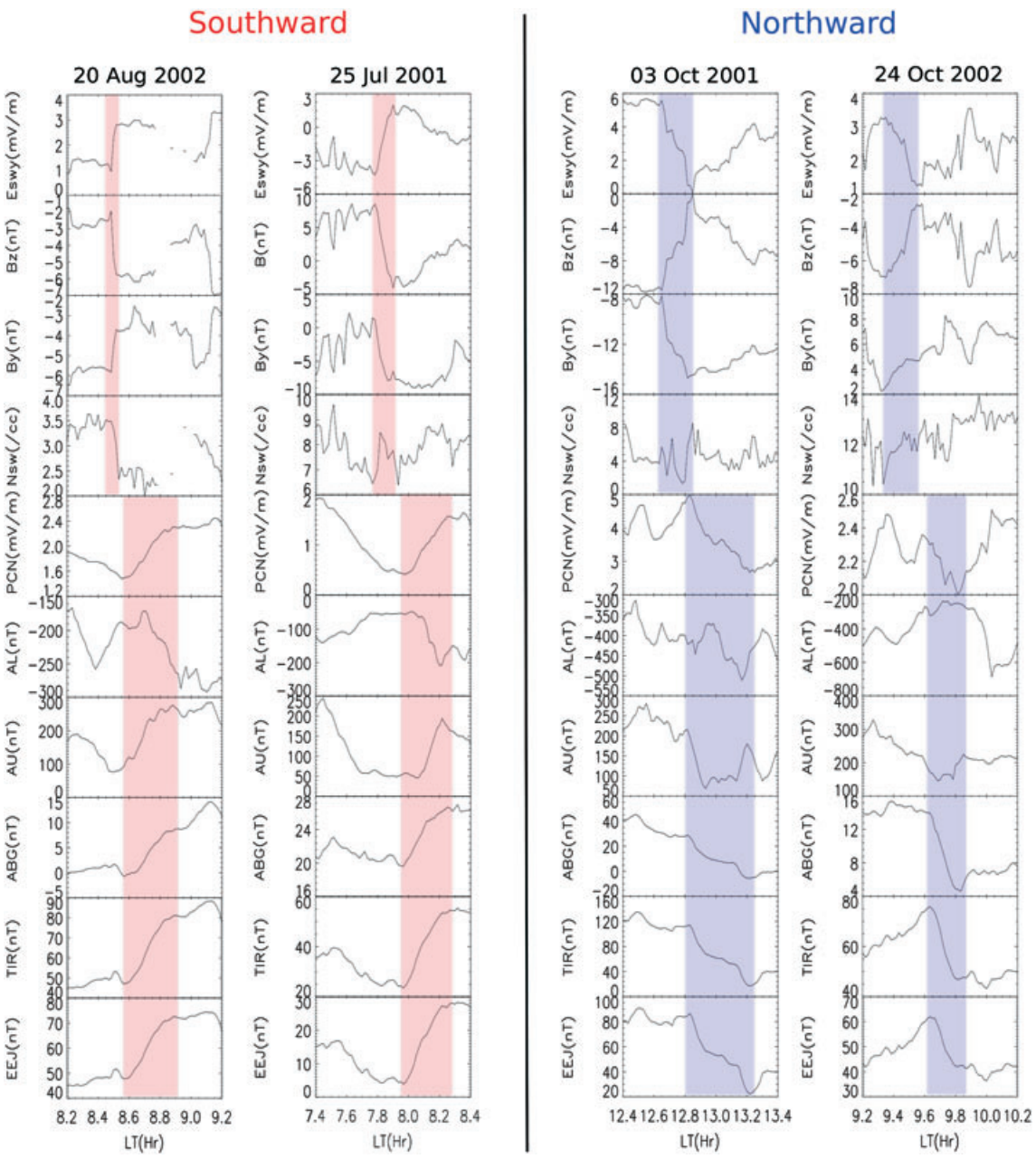

Figure 2. Event signatures observed in different geomagnetic and interplanetary parameters shown for southward (first two left panels) and northward (last two right panels) Bz turnings. For southward/ northward turning, EEJ, ABG, TIR, PCN, AL, and AU generally show enhancement/decrement. The shaded area shows event under consideration.

of convection cells [*Clauer and Friis-Christensen*, 1988; *Weimer*, 1995]. In past studies it has been reported that for northward Bz, two-cell ionospheric convection is formed when $Bz/By < 1$, and four-cell ionospheric convection develops when $Bz/By > 1$ [*Knipp et al.*, 1993; *Cumnock et al.*, 1995]. *Huang et al.* [2000] observed nearly symmetric four-cell convection for $Bz/By \approx 7$, with two normal cells in lower latitudes and two reversed cells in polar cap. *Rastogi and Patel* [1975] reported reversal of electric field during northward IMF turning at the equator using EEJ data, and after that several examples were presented by many researchers [*Patel*, 1978; *Fejer et al.*, 1979; *Kelley et al.*, 2003; *Huang et al.*, 2007; *Wei et al.*, 2011; *Simi et al.*, 2012]. It was thought that westward electric field observed at the equator is dusk-to-dawn IEF, penetrated during northward Bz. However, *Kelley et al.* [1979] proposed different explanation for the transmission during the northward Bz. He emphasized that this electric field originates due to the overshielding electric field. The argument is based on the fact that, though during northward turning reconnection occurs at flanks of the polar cap, it is located in a narrow latitude belt so direct penetration of dusk-to-dawn electric field during northward turning by mapping of the electric field is not efficient. Note that in neither case is the interplanetary electric field mapped to the low latitude directly; rather it maps to high latitude and then transmits to the low latitude. The

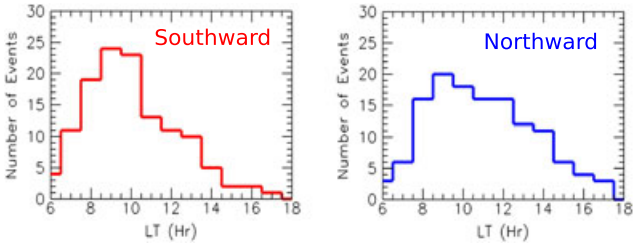

Figure 3. Local time (LT) distributions of events for southward and northward Bz turnings: Both the distributions peak near 9:00 LT showing uneven distribution of identified events with respect to the LT. For northward Bz turnings the distribution looks flatter compare to the event distribution of southward Bz turnings.

inner magnetosphere tries to shield the low latitude from dawn-to-dusk convection electric field by setting up polarization charges (giving rise to dusk-to-dawn electric field) at the inner edge of the ring current [*Kelley et al.*, 1979; *Huang et al.*, 2005; *Wolf et al.*, 2007]. When the shielding electric field is less dominant than the convection electric field, then we observe dawn-to-dusk electric field at the low-latitude ionosphere called as undershielding, whereas when shielding electric field dominates, dusk-to-dawn electric field is observed in the ionosphere called as overshielding. To understand the physical mechanism/mechanisms underlying both cases, it is worth investigating the distinctions and similarities between PPE events associated with northward and southward IMF turnings.

[7] The time delay between the measurements at the satellite located outside the Earth's dayside magnetosphere and ground-based observations consist of six parts as follows: (1) the advection time of the solar wind from the spacecraft to the bow shock nose ($T_{\text{advection}}$), (2) propagation time from the bow shock to the magnetopause ($T_{\text{bs–mp}}$), (3) Alfven transit time along magnetic field lines from the subsolar magnetopause to the polar ionosphere (T_{alfven}), (4) transit time of IEF signature across the magnetosphere (T_{transit}), (5) reconfiguration time of magnetosphere-ionosphere system (T_{reconf}), and (6) propagation time from high latitude to the equatorial ionosphere (T_{transmis}). So total time delay (T_{delay}) observed between the spacecraft and ground measurements can be expressed as

$$T_{\text{delay}} = T_{\text{advection}} + T_{\text{bs–mp}} + T_{\text{alfven}} + T_{\text{transit}} + T_{\text{reconf}} + T_{\text{transmis}} \quad (1)$$

[8] To understand the coupling between magnetosphere and ionosphere, the communication time and ionospheric reconfiguration time are important parameters which are investigated in this paper. The communication time is a time delay between the spacecraft measurements and associated signatures measured at the ground, whereas reconfiguration time is the time taken by the ionosphere to change from one state to another state. The communication time mainly comprises five terms in equation (1) except reconfiguration time. The past studies [e.g., *Lockwood et al.*, 1986; *Todd et al.*, 1988; *Khan and Cowley*, 1999] observed that the onset of the response to Bz changes in the ionosphere first appears near noon and is delayed by increasing amounts toward midnight. However, the studies of *Ridley et al.* [1998], *Ruohoniemi and Greenwald* [1998], and *Murr and Hughes* [2001] have found that the onset of change in the ionospheric flow occurs nearly simultaneously (less than 2 min) across the whole of the ionosphere. *Todd et al.* [1988] studied time scale of the response of the dayside ionospheric flow to the changes in Bz by using Active Magnetospheric Particle Tracer Explorers-United Kingdom Subsatellite and Ion Release Module spacecraft and European Incoherent Scatter "Polar" experiment. They determined the shortest response time delay of 5.5 ± 3.2 min in the early to mid-afternoon sector which increases to 9.5 ± 3.1 min near to the dusk. *Ridley et al.* [1998] observed average of about 8.4 ± 8.2 min communication time from the magnetopause to the ionosphere. For the east-west ionospheric flow *Khan and Cowley* [1999] observed average time delay of 5.4 ± 0.5 min on the dayside, increasing to 11.6 ± 1.4 min on the nightside.

[9] *Murr and Hughes* [2001] studied the ionospheric reconfiguration time by using ground magnetometer data and observed that during sharp north to south transitions of the IMF, the dayside ionospheric convection patterns globally reconfigure themselves with time scale of about 8 min. Also, they reported the most rapid reconfiguration near noon (5 min), and it increases toward night (12 min at 18:00 MLT). *Ridley et al.* [1998] observed an average of 13 min as ionospheric reconfiguration time corresponding to the IMF orientation changes.

[10] We set the main objectives of the present study as to investigate (a) similarities and distinctions between transmitted solar wind electric field signatures to the equatorial region through the currents flowing in the *E* region during

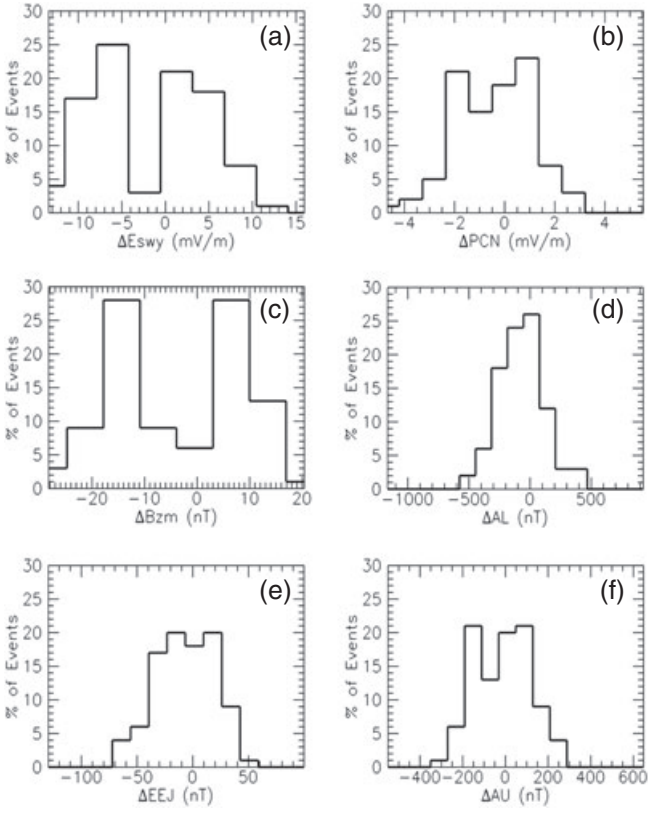

Figure 4. Statistical properties of events: Amplitude histogram of (a) ΔEswy, (b) ΔPCN, (c) ΔBz, (d) ΔAL, (e) ΔEEJ, and (f) ΔAU.

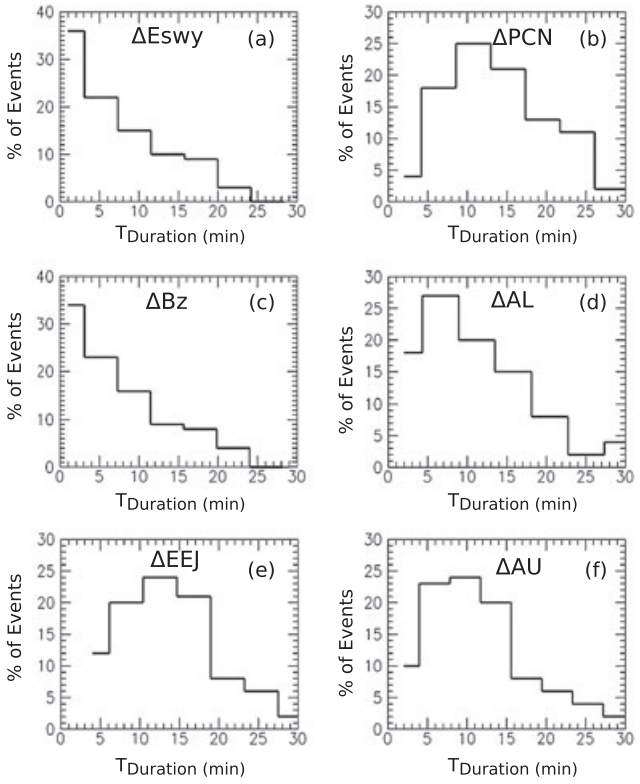

Figure 5. Statistical properties of events: Duration histogram of events associated with (a) ΔEswy, (b) ΔPCN, (c) ΔBz, (d) ΔAL, (e) ΔEEJ, and (f) ΔAU.

southward and northward Bz turnings, (b) local time dependence of equatorial ionospheric signatures of the transmitted electric field and its efficiency, (c) statistical characteristics of event parameters, (d) relationship between Eswy turnings and associated EEJ changes, and (e) high-latitude indices and their interrelationships during PPE. The paper is arranged as follows: Section 2 describes the data and adopted methodology for the selection of events in the present investigation. Section 3 gives the statistical characteristics of studied events. The magnetospheric communication time and ionospheric reconfiguration time are discussed in section 4. Section 5 presents the local time variation of the EEJ amplitudes for northward and southward Bz turnings. Section 6 presents the correlation and linear regression analysis. Section 7 ends the paper with discussions and conclusions inferred from the present study.

2. Database and Selection of Events

[11] The enhanced ionospheric conductivity in the equatorial region amplifies the magnetic field signatures of transmitted high-latitude electric fields. It is suggested and shown by *Rastogi and Klobuchar* [1990] that the strength of the daytime equatorial electrojet (EEJ) could be measured using two magnetometers, one situated near dip equator and the other located at 6° to 9° away from the dip equator. EEJ index is computed by doing local midnight correction for each station and then by subtracting simultaneous observations of magnetic field at two observatories. The derived EEJ index is a good proxy for the state of the equatorial ionosphere. The EEJ index can be used to study the characteristics of the transmitted fields to the equator mainly during daytime.

[12] We have used 1 min temporal resolution data of horizontal component of the geomagnetic field from Indian stations, Alibag (ABG, geomagnetic latitude 10.36°) and Tirunelveli (TIR, geomagnetic latitude 0.03°). Alibag is situated away from the EEJ influence, while TIR is very close to the magnetic equator, so one can get good estimate of EEJ strength. The Indian Institute of Geomagnetism, India, routinely computes the EEJ index which is used in the present study. We have identified the events from five most disturbed days of each month of years 2001–2005. The period mainly covers the peak and descending phases of solar cycle 23. Geomagnetic disturbances are mainly controlled by sheath and magnetic clouds during this period which are drivers of PPE [*Gonzalez et al.*, 2011; *Guo et al.*, 2011]. As compared to the dayside equatorial conductivity, the nighttime conductivity is less than 20% [*Abdu et al.*, 2007; *Tsuji et al.*, 2012]. This justifies the difficulties in observations of nighttime PPE in equatorial magnetometer data, and so the present study is constrained to the daytime hours (06:00–18:00 LT).

[13] For the interplanetary conditions, we have used 1 min averaged definitive time-shifted multispacecraft interplanetary magnetic field and plasma data, obtained from OMNI database at Coordinated Data Analysis Web (http://cdaweb.gsfc.nasa.gov/). The data are time shifted from the spacecraft location to the Earth's bow shock nose. Solar wind parameters like density (Nsw), dynamic pressure (Psw), Bz, and eastward component of IEF (Eswy) were studied for the identified events. The Eswy is a component of solar wind electric field along the *y* axis (eastward) in GSM coordinate system. The auroral activity indices AL (amplitude lower) and AU (amplitude upper) were obtained from World Data Center, Kyoto. The polar cap index (PCN) used for the present analysis is derived from Thule station located in the northern polar cap. It is important to note that EEJ index

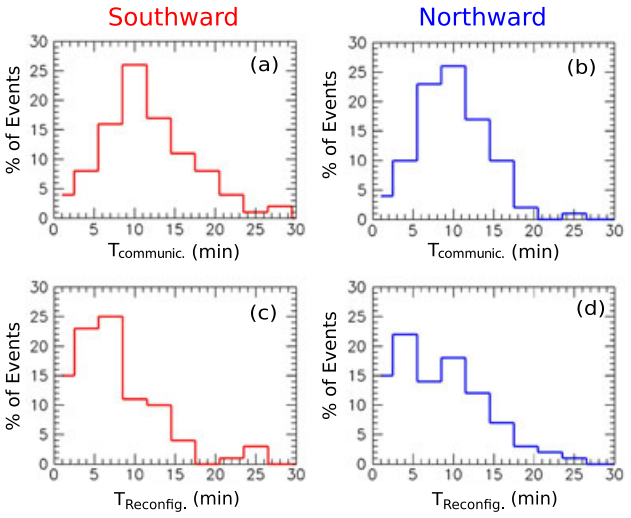

Figure 6. (upper panel) Communication time between Earth's bow shock nose and the equator (T_{Communic}) for (a) southward and (b) northward Bz turnings; (lower panel) ionospheric reconfiguration time (T_{Reconfg}) for (c) southward and (d) northward Bz turnings.

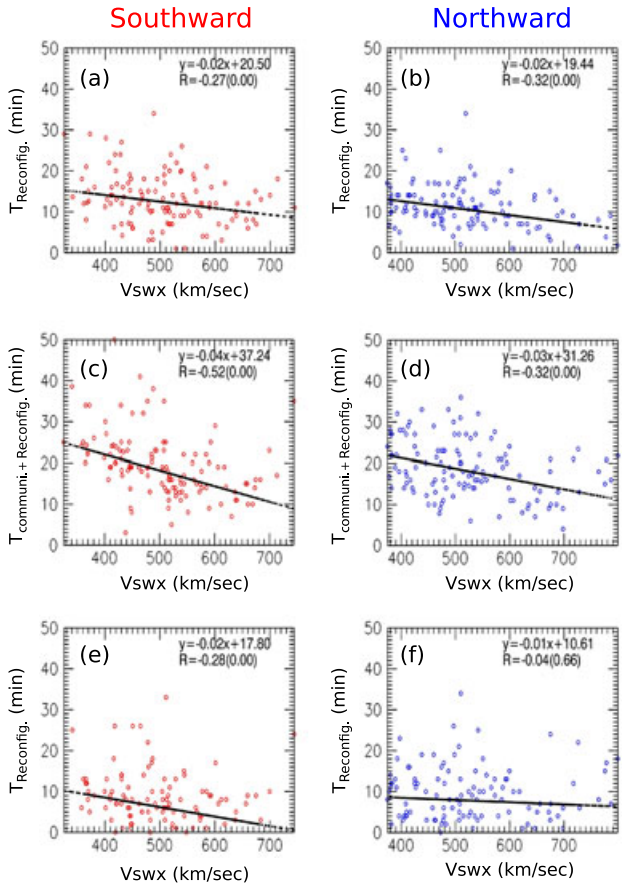

Figure 7. Linear relationship of radial solar wind velocity (Vswx) with (a, b) time delay from start of IMF turning to the start of corresponding EEJ signature ($T_{\text{Communic.}}$), (c, d) time delay from end of IMF turning to end of the corresponding EEJ signature ($T_{\text{Communic.+Reconfg.}}$), and (e, f) ionospheric reconfiguration time ($T_{\text{Reconfg.}}$).

can represent the strength of disturbance in the equatorial ionosphere; AL and AU indices indicate auroral disturbance level and a good proxy for high-latitude geomagnetic activity, whereas PCN index represents the geomagnetic activity in the polar cap region [*Troshichev and Andrezen*, 1985; *Troshichev et al.*, 1988; *Troshichev et al.*, 2006]. So we can study the signatures of sudden Bz turnings in polar, auroral, and equatorial ionosphere simultaneously. Since the variations in solar wind dynamic pressure have significant impact on the geomagnetic field variations recorded on the ground, in order to eliminate this effect, we selected the PPE events when the solar wind dynamic pressure variations are nonsignificant (< 3 nPa).

[14] Figure 1 shows a temporal variation of the EEJ and *H* component at ABG and TIR along with high-latitude indices and interplanetary parameters on 1 August 2002, one of the studied disturbed days. The dotted line represents the average of *H* component on five quiet days for the month of August 2002. The EEJ index (bottommost plot of Figure 1) shows the enhanced variations between 10:00 and 12:30 LT (shown by shaded area) which is well correlated with the variations seen in the PCN, AL, and AU indices and Bz and Eswy, whereas at the same time solar wind density (Nsw) showed very small variation. Thus, it can be seen that the high-frequency fluctuations riding on diurnal variation in the geomagnetic field variations in the Indian zone are correlated with the fluctuations seen in Bz, Eswy, AL, AU, and PCN. The associated changes in IMF and geomagnetic parameters were noted for each event.

[15] When the observed sharp increase (decrease) in EEJ index and *H* component of TIR and ABG is associated with the sharp southward (northward) Bz turning, only then it is labeled as an event. As a convention we have termed Bz changes as northward turnings when Bz has changed from south to north or there is reduction in southward component of Bz. Similarly, turnings are termed as southward when Bz changed from north to south or there is a reduction in northward component of Bz. We have identified events using 3 h time window in which Bz turnings are followed by EEJ signatures. The preliminary selection of events uses the following criterion. We have selected only those Bz turnings which take place during Indian daytime for which change in Bz is greater than 2 nT, the duration of Bz turning is between 2 and 25 min and which are not accompanied with sharp changes in the solar wind dynamic pressure (< 3) nPa. The events are selected by visual inspection where sharp changes in Bz are associated with sudden increase (or decrease) in the EEJ index. The identified events exhibit a minimum threshold of 7 nT for the response in EEJ index. The amplitude of Bz change and associated signatures seen in indices is estimated by taking the difference between the average of 3 min values before the onset and maximum/minimum value observed just after the onset of the event. Note that for the present study, we have selected only those Bz sudden turnings which occur during daytime (06:00–18:00 LT) of Indian region (LT = UT +5 h) and whose response is detectable in the magnetic field variations at ABG, TIR, and EEJ index. There were Bz turnings which did not show signatures in EEJ, ABG, and TIR. It is observed that the Bz turnings of small amplitude which occur near dawn or dusk do not show signatures in EEJ, ABG, and TIR. This could be due to the less ionospheric conductivity during that time. About 50% of southward and 65% of northward Bz turnings showed signatures in EEJ and *H* component magnetic field variation at ABG and TIR during local time range 10–14 h. When the events having change in Bz > 3 nT are considered, then the percentage of signatures seen in EEJ increased to 57% for southward turnings and to 72% for northward turnings indicating higher Bz amplitude events are more efficient to cause detectable EEJ signatures. It should be noted that the signatures in EEJ index are considered only when they are detectable by visual inspection. From observations we postulate that, if the rate of change of magnetic field variation in EEJ index due to Bz turning is less or not significantly larger than the rate of change of background magnetic field variations due to normal diurnal pattern of EEJ or H variation, then it is not possible to detect easily response signature in the EEJ index. Using the above stated criterion, a total of 250 (125 events as northward turning and remaining 125 as southward turnings) events during 2001–2005 were identified and analyzed.

[16] Figure 2 demonstrates the selection of events during northward and southward Bz turnings. The sample events are shown for southward and northward turnings of Bz separately. The shaded area shows identified events in the interplanetary parameters and various ground-based indices.

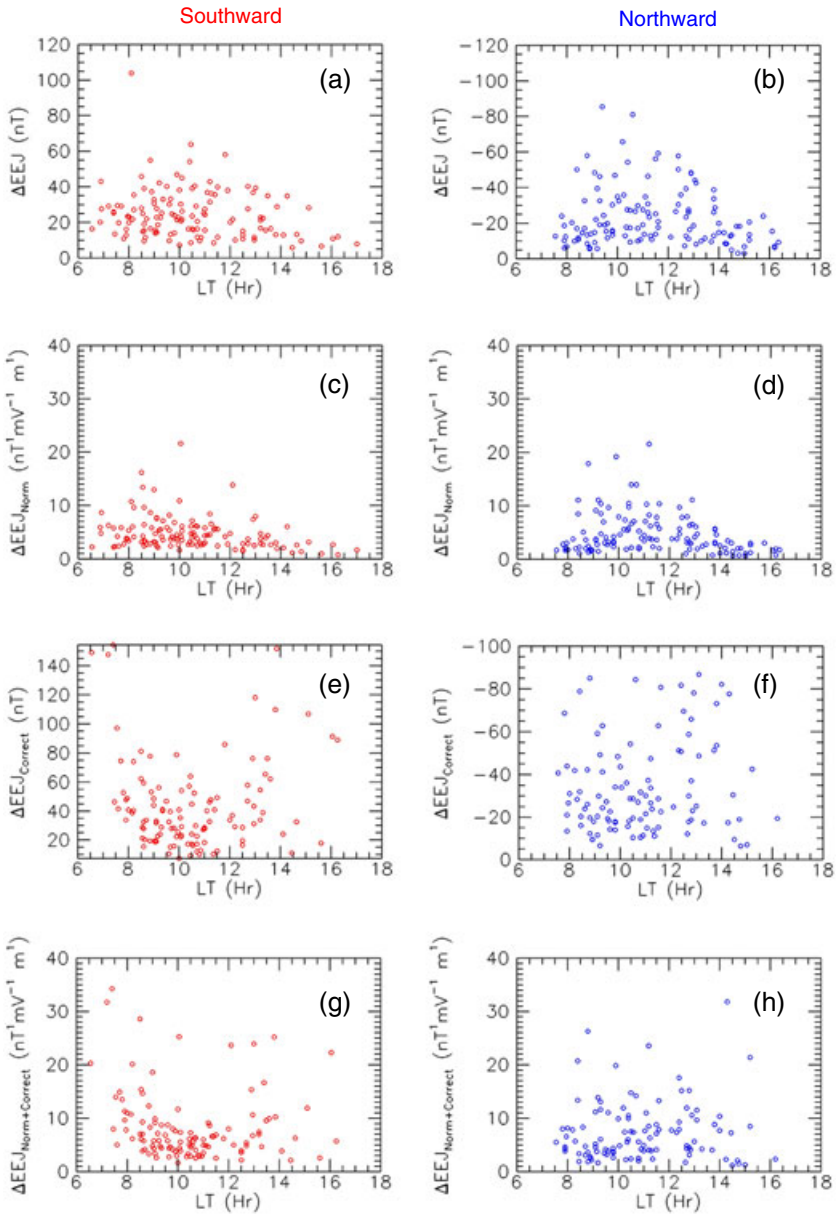

Figure 8. Local time dependence EEJ response to Bz turnings. (a, b) Amplitude of events seen in EEJ (ΔEEJ) without any correction of conductivity or normalization by Eswy; (c, d) ΔEEJ is normalized by associated changes in Eswy (ΔEswy); (e, f) ΔEEJ is corrected for conductivities (see the text for details); and (g, h) ΔEEJ is corrected for conductivity and then normalized by ΔEswy.

For southward turnings of Bz (i.e., enhancement in eastward electric field Eswy) it is observed that EEJ and *H* component measured at ABG and TIR increase almost simultaneously. The magnitude of response in *H* component at TIR is greater than ABG which is due to the enhanced cowling conductivity at the equator. The PCN index which represents polar cap electric field shows similar enhancement. Also, AL and AU indices show the change during the event; both show the enhancement in the strength. Since AL index represents westward current (negative), it appears opposite to AU (eastward current). During northward turning of Bz (right side plots), EEJ and *H* component at ABG and TIR show decrement. The signatures in AL and AU indices are not very clear during northward turnings, but generally they show decrement indicating weakening of auroral electrojet currents during northward turnings of Bz. For both the cases of Bz turnings the response to the sudden Bz changes seen in the ground geomagnetic parameters is not simultaneous; often ground response is delayed by a few minutes with respect to the observations at the nose of the Earth's bow shock, which is discussed in detail in section 4. The transition duration of Bz signatures in ground-based magnetic field measurements is greater than Bz transition duration. The response is almost simultaneously (less than 1 min) recorded at the polar, auroral, and equatorial regions. This indicates almost instantaneous transmission of high-latitude electric field to the equator. The cross-correlation coefficients between the signatures seen in EEJ and PCN are 0.99,

Table 1. Correlation Coefficients for Southward Turning Events (10:00–14:00 LT)

	$\Delta EEJ_{Correct}$	ΔPCN	ΔAL	ΔAU	ΔEswy	ΔBz	ΔBy	ΔPsw
$\Delta EEJ_{Correct}$	1.000	0.321	**0.416**	0.077	**0.460**	**–0.512**	–0.238	–0.065
ΔPCN		1.000	**0.452**	0.397	**0.490**	**–0.529**	–0.083	0.081
ΔAL			1.000	0.312	0.390	–0.279	–0.355	0.179
ΔAU				1.000	**0.560**	–0.339	–0.390	0.134
ΔEswy					1.000	**–0.908**	–0.233	0.040
ΔBz						1.000	0.147	–0.089
ΔBy							1.000	–0.146
ΔPsw								1.000

Table 2. Correlation Coefficients for Northward Turning Events (10:00–14:00 LT)

	$\Delta EEJ_{Correct}$	ΔPCN	ΔAL	ΔAU	ΔEswy	ΔBz	ΔBy	ΔPsw
$\Delta EEJ_{Correct}$	1.000	0.375	0.327	0.126	**0.590**	**–0.503**	0.103	0.203
ΔPCN		1.000	**0.441**	0.375	**0.450**	**–0.518**	–0.046	0.043
ΔAL			1.000	0.256	**0.400**	–0.258	–0.228	0.040
ΔAU				1.000	0.150	0.054	–0.222	–0.098
ΔEswy					1.000	**–0.850**	–0.081	0.183
ΔBz						1.000	0.083	0.115
ΔBy							1.000	–0.071
ΔPsw								1.000

0.95, 0.91, and 0.91 for 20 August 2002, 25 July 2001, 03 October 2001, and 24 October 2002 events, respectively.

3. Statistical Characteristics

[17] To find probability distribution, a histogram technique is used as it is an easy method for nonparametric statistics. The histograms of amplitude and duration are plotted for all events. Choosing bin size is one of the important things in histogram analysis. If one uses large bin size, the histogram becomes smooth so details of the information are lost. Also, if smaller bin width is used, then the histogram becomes rough and it appears more noisy. The optimum bin width has to be chosen to get true probability distribution. We use relationship $w = 3.49\sigma N^{-1/3}$ derived by *Scott* [1979], where w is bin width, N is number of events, and σ is standard deviation of data.

[18] The local time (LT) distribution of studied events is shown in Figure 3 for northward and southward Bz turnings separately. It shows the maximum events selected were from LT ranging from 9 to 10 h. About 82% of events lie in the LT range between 8 and 14 h when the equatorial ionosphere conductivity is high and it is possible to detect the response signature in the EEJ index. Few events are identified in the evening hours during both the cases of IMF turnings. Both the distributions peak near 9:00 LT showing uneven distribution of identified events with respect to the LT. For northward Bz turnings the distribution looks flatter compared to the event distribution of southward IMF turnings.

[19] The amplitude distributions of ΔEEJ, ΔAL, ΔAU, and ΔPCN along with associated ΔEswy and ΔBz distributions are shown in Figure 4. Most of the events have response amplitude of approximately within ±50 nT for EEJ, ±300 nT for AL, and ±200 nT for AU. The amplitude of Eswy changed within ±10 mV/m, whereas PCN lay within ±2 mV/m. Bz turnings show amplitude variation within ±20 nT. Except for ΔAL, the negative amplitudes of ΔEEJ, ΔPCN, and ΔAU are normally associated with the northward Bz turnings, and positive amplitudes are associated with the southward Bz turnings. Since AL is a proxy for the westward current, positive changes in AL are associated with the northward Bz turnings and negative amplitudes of ΔAL to the southward Bz turnings. The distributions of all parameters show asymmetry for northward and southward Bz turnings.

[20] Figure 5 represents histograms of the durations of events. Duration of event is defined as a time interval of the change seen in observed parameter for all studied events. The histogram is plotted for all events irrespective of Bz turning. It can be observed from Figures 5b, 5d, 5e, and 5f that there are preferred average time scales for the time durations associated with ΔPCN, ΔAL, ΔEEJ, and ΔAU, whereas durations corresponding to ΔBz or ΔEswy (Figures 5a and 5c) turnings do not show any preferred time scale. Around 70% of Bz turning events have time duration between 2 and 10 min. The number of events increases with shorter duration for ΔBz or ΔEswy which might be indication of the self-organized criticality (SOC) of the solar wind [*Bak et al.*, 1987]. In the critical state, the system has a distribution of minimally stable regions of all sizes so that small perturbations give rise to avalanches of all sizes from the smallest possible avalanche up to the size of the system. The characteristics of the SOC system is that no preferred scale exists [*Lu and Hamilton*, 1991]. But it is important to note that geomagnetic parameters exhibit some preferred time scales as seen in Figures 5b, 5d, 5e, and 5f.

4. Magnetospheric Communication and Ionospheric Reconfiguration Time

[21] The IMF data used in the present study are time shifted to bow shock nose which is obtained from OMNI database. The details of the time-shift technique is elaborated at http://omniweb.gsfc.nasa.gov/html/HROdocum.html. The ground-based signatures related to the Bz turnings are not seen simultaneous with Bz due to additional

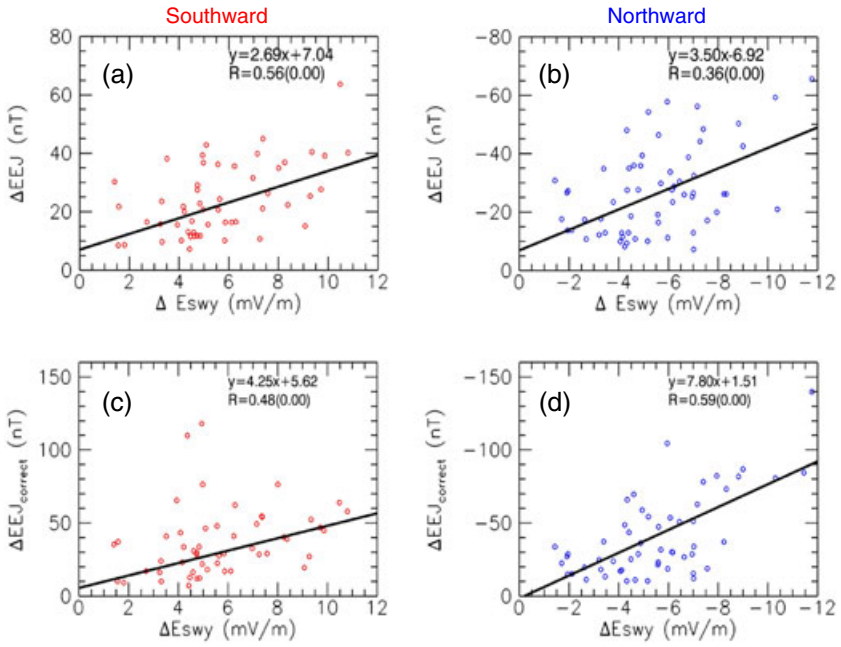

Figure 9. (upper panels) The relationship of ΔEEJ and associated ΔEswy. (lower panels) Conductivity-corrected ΔEEJ ($\Delta EEJ_{Correct}$) relationship with corresponding ΔEswy (left panels represent southward turnings events and right panels northward turning events).

communication time associated with the propagation from the bow shock nose to the ionosphere. It is inferred from Figure 5 that the time duration of ΔEswy and ΔBz do not show any preferred time scale, whereas durations of ΔPCN, ΔAL, ΔAU, and ΔEEJ show preferred time scales. This may indicate that the time scales associated with magnetosphere-ionosphere system are responsible for the observed preferred time scales. This time duration is composed of different propagation and transition times as discussed in section 1. Here, we define the communication time as time between start of the Bz turning observed at bow shock nose and the onset of the signature at the ionosphere. Thus, we concentrate on the time delay seen for the initial change (or very first change) between bow shock and ground. *Khan and Cowley* [1999] reported that the travel time from bow shock to magnetopause (or magnetosheath transit time) is less than 1 min.

[22] For sharp Bz changes the response of the magnetosphere-ionosphere system is expected to be gradual due to its inertia which can be represented by ionospheric reconfiguration time. So another quantity, called the reconfiguration time, is the time that the ionosphere takes to transit from one state to another state during the sharp Bz turnings. Estimating this time is a little tricky. In literature, the ionospheric reconfiguration time is defined as the time interval of the ionospheric change (= time of the final change – time of the start of change). However, we think that this definition includes the time interval of the Bz change itself (seen at the bow shock), and hence it is required to remove it in order to define the ionospheric reconfiguration time. So we estimate reconfiguration time by subtracting ΔEswy duration from the duration of ΔEEJ which can be represented by the following equation.

$$T_{\text{Reconfig.}} = (T_{\text{duration}})_{\Delta EEJ} - (T_{\text{duration}})_{\Delta Eswy} \quad (2)$$

The first term in the right-hand side of equation (2) represents time duration of ΔEEJ, whereas the second term represents duration of ΔEswy. Figure 6 shows the statistical study of communication time and reconfiguration time for studied events. As shown in Figures 6a and 6b, the communication time was studied for northward and southward Bz turnings separately, and it is found that the mean time for the signature to communicate from bow shock nose to equatorial ionosphere is about 13 ± 6 min for Bz southward turnings and about 11 ± 5 min for Bz northward turnings, where error indicates the standard deviation of samples. So on an average we observe approximately 12 min communication time (from bow shock nose to the ionosphere) which shows very good consistency with the past studies mentioned in section 1. We also notice almost the same communication time observed for polar ionosphere (not shown in the figure) indicating short inter-ionospheric communication time, i.e., fast propagation of polar electric field to the equator. We do not see any LT dependence of communication time (not shown here) within the presently analyzed range of 06:00 to 18:00 LT.

[23] The observed equatorial ionospheric (Figure 6c) average reconfiguration time for southward turning is 9 ± 6 min and for northward turning (Figure 6d) is 11 ± 8 min. Also, it is important to note that the distribution of reconfiguration time differs for southward and northward Bz turning events; it is more widely distributed for northward as compared to southward Bz turnings.

[24] Further, we examine the dependence of these communication and reconfiguration times on the Earth-directed radial component of the solar wind velocity (Vswx), depicted in Figure 7. It can be noticed that the observed communication time is inversely proportional to the solar wind flow (Figures 7a and 7b). The correlation and linearity is nearly equal for both the turnings of Bz. Time of

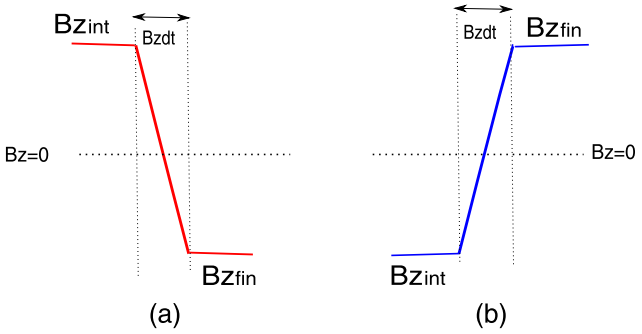

Figure 10. Schematics of (a) southward and (b) northward Bz turnings (see text for details).

sweeping of discontinuity across the magnetosphere by solar wind might be responsible for high anticorrelation of time delay with Vswx. It is expected that the faster solar wind flow crosses the magnetosphere in shorter time. So this can explain the observed anticorrection of communication time with Vswx. The middle panel shows the better correlation of Vswx with the time delay computed from the end of the sharp turning of Bz to the corresponding final changed state of the ionosphere which includes both communication and ionospheric reconfiguration time (Figures 7c and 7d). Figures 7e and 7f display the scatter plot between Vswx and reconfiguration time computed using equation (2) during southward and northward turnings. A fairly good anticorrelation between Vswx and reconfiguration time is evident during southward Bz turning, but almost no correlation is seen for northward Bz turnings. This is a very important observation, since it suggests that solar wind velocity plays a role in the reconfiguration time during southward Bz turnings but not during northward Bz turnings.

5. Local Time Dependence

[25] Though our selection of events are constrained to the daytime, a larger number of events are in the prenoon hours (Figure 3). A maximum number of events are observed near 9:00 LT, and the number decreases toward dawn and dusk for both southward and northward turning events. Figures 8a and 8b show the LT variation of the ΔEEJ during southward and northward Bz orientations, which show maximum magnitude near diurnal peak of EEJ; this suggests strong influence of diurnal variation of EEJ. The normalized amplitude of ΔEEJ with respect to the associated change in Eswy (ΔEswy) is shown in Figures 8c and 8d, yet LT dependence

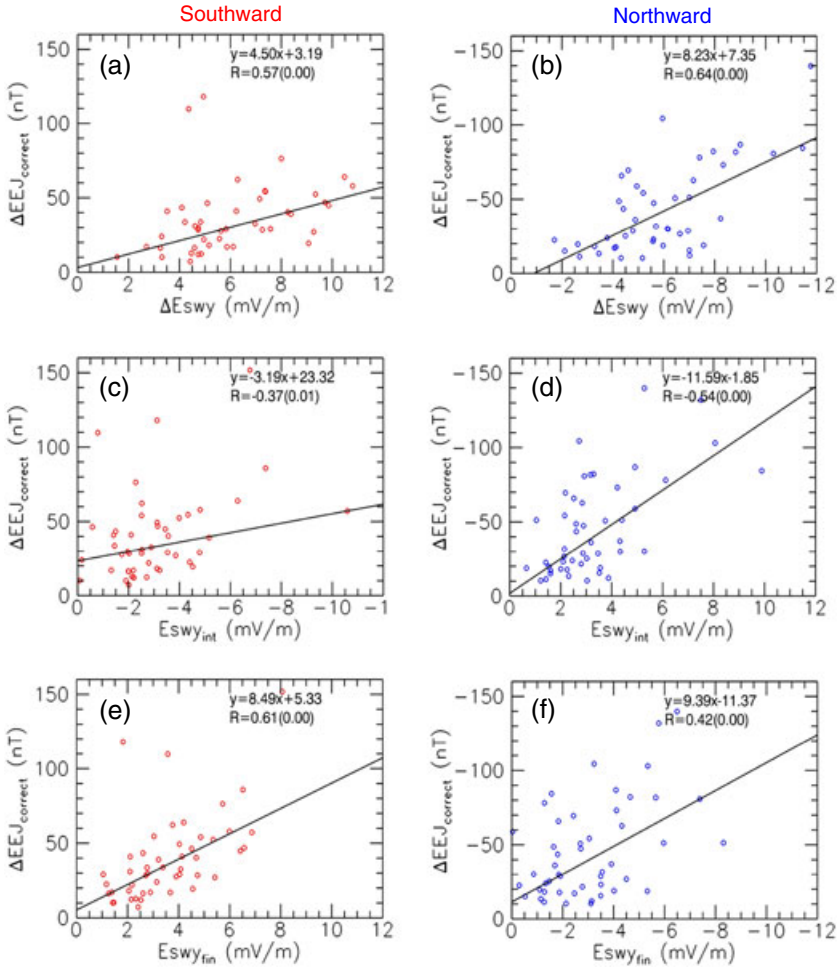

Figure 11. Linear relationship of $\Delta EEJ_{Correct}$ with (a, b) net change of Eswy during turning (ΔEswy) Considering Bz turning, crossing zero, (c, d) magnitude of turning estimated from start to zero ($Eswy_{int}$), (e, f) magnitude of turnings estimated from zero to end value ($Eswy_{fin}$).

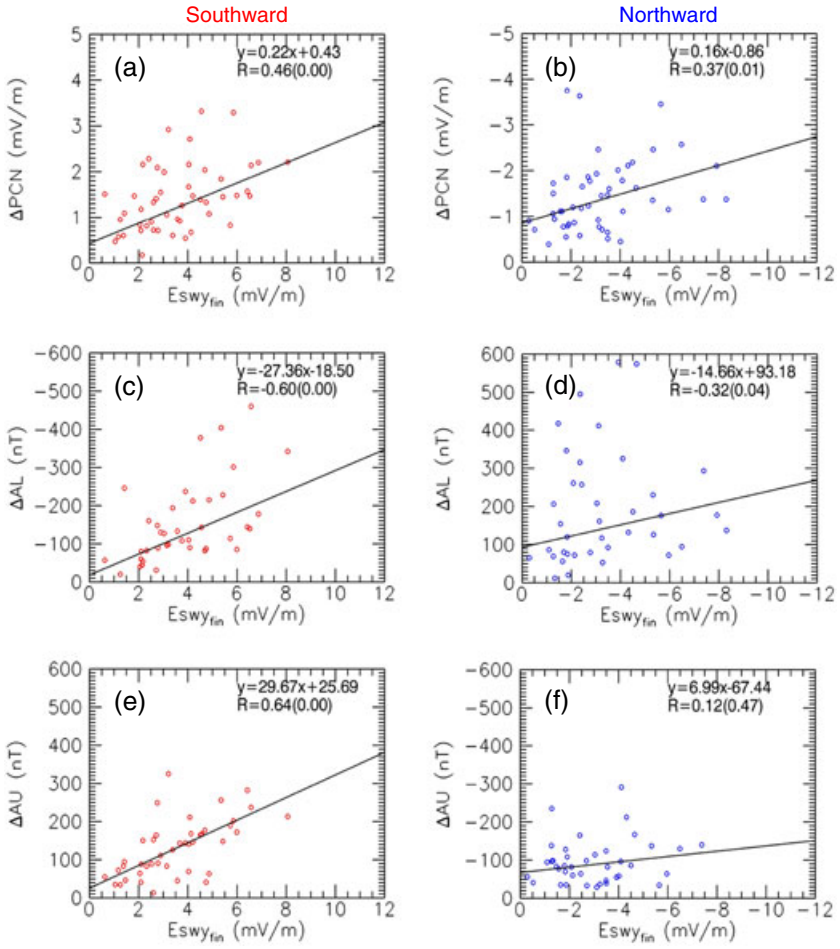

Figure 12. Linear relationship for ΔPCN, ΔAL, and ΔAU with associated Eswy amplitude estimated from zero to final value Eswy$_{fin}$.

is seen which is due to the diurnal variation of the equatorial ionospheric conductivity. To remove conductivity effect, correction to ΔEEJ is done by using multiplication factor $(EEJ_{peak})_{qavg}/EEJ(t)_{qavg}$. Where $(EEJ_{peak})_{qavg}$ is the peak value of EEJ obtained by averaging five quiet days of the month, and $EEJ(t)_{qavg}$ is the five quiet day average EEJ value at the corresponding LT of the event. Figures 8e and 8f demonstrate the LT variation of conductivity-corrected EEJ signatures ($\Delta EEJ_{Correct}$) for southward and northward turnings. It can be seen that there is a complete scatter, so no LT dependence seen assuring the diurnal variation of the conductivity effect has been eliminated, and the applied conductivity corrections are reasonable. These conductivity-corrected EEJ variations are used for the linear regression analysis performed in section 6. The LT variation of conductivity-corrected and Eswy-normalized ΔEEJ ($\Delta EEJ_{Norm+Correct}$) shows broad scatter, and also the peak near local noon has vanished (Figures 8g and 8h).

6. Correlation and Linear Regression Analysis

[26] Correlation and linear regression analysis is performed to understand the relationship between Bz turnings and associated signatures seen in various geomagnetic parameters. Spearman's correlation coefficient was estimated with two-sided significance of its deviation from zero. The studied LT range is divided into three sectors 06:00–10:00, 10:00–14:00, and 14:00–18:00 LT. The best correlation is seen for 10:00–14:00 LT sector so here we present analysis of events falling on 10:00–14:00 LT. The coefficients which are significant (> 99% confidence level) are shown in bold letters; refer to Tables 1 and 2 for details. It is important to note that the correlation between solar wind pressure changes ΔPsw and other parameters is low, assuring less dependence of events on the pressure changes due to the selection criteria for events. The correlation of conductivity-corrected EEJ ($\Delta EEJ_{Correct}$) with ΔEswy (and ΔBz) is high for both Bz turnings. For southward turnings, ΔEswy and ΔAU are better correlated as compared to northward turnings. There is a positive correlation observed between ΔEswy and ΔPCN for both the turning events. ΔEswy and ΔBz show high anticorrelation which is expected.

[27] Linear regression analysis is performed to establish relationship between different parameters by using absolute linear fit. Since absolute fit is less sensitive to outliers, we chose it over least square fit. Figure 9 shows the linear relationship of ΔEEJ and $\Delta EEJ_{Correct}$ with ΔEswy. The correlation coefficient (R) and straight line equation are shown for each scatter plot. The term shown in brackets after the R value is a significance value of estimated correlation. As compared to ΔEEJ, the $\Delta EEJ_{Correct}$ shows better correlation

with ΔEswy for northward Bz turnings, when southward Bz turnings linearity is almost the same. The linear regression shows a nonzero *y* intercept. This might indicate the contamination of the estimated amplitudes by the background field. Further detailed studies are needed to determine the cause of the nonzero intercept.

[28] It is important to note that the amplitudes of Bz (ΔBz) are determined by considering the start of the sharp change to the end of it. We now concentrate on the events in which Bz has changed the sign, i.e., when Bz crosses zero (Figure 10). When one considers the situation as depicted in Figure 10, for southward turning, initial Bz (Bz_{int}) is northward and final Bz (Bz_{fin}) is southward. Likewise for northward turnings, initial Bz is southward and final Bz is northward. For these events one can write $\Delta Bz = |Bz_{int}| + |Bz_{fin}|$ and $\Delta Eswy = |Eswy_{int}| + |Eswy_{fin}|$. Now we investigate linear regression and correlation of geomagnetic signatures with $Eswy_{int}$ and $Eswy_{fin}$ separately (Figure 11). The left panels of Figure 11 present southward turning events, whereas northward turning events are shown in the right panels. Note that the plots in Figures 9c and 9d consider all the events including those not crossing zero level of Bz. The correlation has improved in Figures 11a and 11b, when only those events are considered for which Bz has crossed zero level. The scatter plots between $\Delta EEJ_{Correct}$ and initial value of Eswy, i.e., $Eswy_{int}$ show better correction for northward as compared to southward turnings (Figures 11c and 11d). Also, it is interesting to note that when the magnitude of turning is estimated from zero to final $Eswy_{fin}$, the correlation is better for southward as compared to the northward turnings (Figures 11e and 11f). The southward turning events show stronger correlation and less scatter with $Eswy_{fin}$ as compared to northward turning events, indicating asymmetry in both types of turnings. The physical significance of this asymmetry is elaborated in the discussion part of this paper. Similarly, correlation of ΔPCN, ΔAL, and ΔAU signatures with $Eswy_{fin}$ is depicted in Figure 12. Note that here we do not display the plots for $Eswy_{int}$ because no clear relationship is observed for those. It can be seen that a clear difference between southward (left panel) and northward (right panel) events exists. The R^2 values for AL and AU are significantly higher for southward events (0.36 for AL and 0.41 for AU) compared to those during northward turnings (0.10 for Al and 0.01 for AU). The PCN shows nearly equal R^2 for both Bz turnings.

7. Summary and Discussion

[29] The present work aims to understand the differences in characteristics of geomagnetic field response of PPE associated with northward and southward turnings of the Bz through the statistical analysis of PPE events identified during 2001–2005. We observe sharp increase/decrease in the EEJ index corresponding to the sudden southward/northward turnings of Bz. It is noted that the response signature in the PCN index is similar to that in the EEJ index, resulting in significantly high correlation coefficient between two signatures (> 0.9), whereas signatures in AL and AU are not always consistent in terms of continuous increase or decrease. The auroral indices are influenced by the substorm activity and high-latitude current systems which can distort the signatures of sudden Bz turnings significantly. The signatures in PCN and EEJ indices seem to be simultaneous, within a minute. Thus, it indicates the prompt penetration of the signature from the polar latitude to the equatorial region.

[30] We observe approximately 12 ± 6 min communication time of Bz signature from bow shock nose to the ionosphere which is comparable to the optimum propagation time of 17 min to travel from the magnetosphere's bow shock nose to the equatorial ionosphere reported by *Manoj et al.* [2008]. The inverse proportionality between communication time and solar wind speed might indicate the crossing of the magnetosphere by the solar wind discontinuity. When solar wind plasma passes through bow shock, it decelerates and becomes nearly zero at the subsolar point. The plasma in magnetosheath flows along the surface of the magnetopause toward the polar region. Considering radial solar wind speed (Vswx) equal to 500 km/s and subsolar magnetopause distance as 10*Re* (*Re* = radius of the earth) and if we assume in magnetosheath solar wind decelerates to speed approximately 1/4 of Vswx (as suggested by *Khan and Cowley* [1999]), then the travel time for the solar wind electric field signatures to propagate in quarter sphere in order to reach the poles would be approximately 13 min, which is very close to the observed communication time.

[31] The ionosphere has its inertia which results in a finite response time to the sudden external changes applied to the ionosphere. This response time is termed as ionospheric reconfiguration time. Approximately 10 ± 8 min of ionospheric reconfiguration time is observed for all events. For southward Bz turnings, the reconfiguration time is found to be inversely dependent on Vswx, while northward Bz turnings do not show such dependence. This is intriguing as dependence of reconfiguration time on solar wind speed is not obvious and needs more detailed study to understand its implications. This might throw some light on the differences in physical mechanisms involved in magnetosphere-ionosphere coupling during southward and northward turnings. Also, one can postulate that ionospheric reconfiguration time should depend on the thickness and orientation of the discontinuity which can be investigated in future studies.

[32] It is important to examine the local time dependence of the penetration. The observed LT dependence of the PPE signatures in EEJ essentially includes the diurnal variation of enhanced cowling conductivity at the equator. The amplitudes of PPE in *H* component of ABG shows weaker LT variation as compared to those seen at TIR, which is expected. After removing the conductivity effect, almost no LT dependence is seen in $\Delta EEJ_{Correct}$.

[33] The correlation between $\Delta EEJ_{Correct}$ and ΔEswy is excellent and significant up to 99% during southward and northward Bz turnings. The correlation of $\Delta EEJ_{Correct}$ with ΔPCN, ΔAL, and ΔEswy is almost the same for southward and northward Bz turnings. The correlation of ΔAU with ΔEswy is very strong for southward as compared to northward Bz turnings. This is due to the enhanced magnetospheric convection during the southward Bz. It is observed that the linear relationship between conductivity-removed PPE amplitudes ($\Delta EEJ_{Correct}$) and ΔEswy differs for northward and southward turnings. The estimated linear absolute fit for southward Bz turnings is $\Delta EEJ_{Correct} = 4.50 \times \Delta Eswy + 3.19$, whereas for northward Bz turnings

$\Delta EEJ_{Correct} = 8.23 \times \Delta Eswy + 7.35$. This shows that slope for northward turning events is higher as compared to the southward turnings which indicates higher efficiency of PPE during northward turnings. These observations can be compared with the least square fit values between ΔH and $E \times B$ drift estimated from Jicamarca Incoherent Scatter Radar (ISR) data [*Anderson et al.*, 2002]. It is important to note that they studied the relationship between ionospheric $E \times B$ drifts and strength of EEJ, whereas the present work investigates the relationship between sharp changes in Eswy and its signatures in EEJ. The F region $E \times B$ drifts are controlled by ionospheric zonal electric fields. Upward ionospheric drifts correspond to the eastward (dawn to dusk) electric fields, whereas downward drifts are mainly due to the westward (dusk to dawn) electric fields. It has been reported that rapid variations in $E \times B$ drift can be related to the PPE and hence to Eswy. *Anderson et al.* [2002] found linear fit of $\Delta H = 2.3\, E \times B$ drift + 14.0 nT when both ΔH and $E \times B$ drifts were positive, whereas relationship is $\Delta H = 6.1\, E \times B$ drift – 11.0 nT when both were negative. Thus, slope in linear fit is higher for downward $E \times B$ drifts than that for upward drifts and indicate higher efficiency for dusk-to-dawn electric field. Our study also shows similar results, i.e., when ΔEEJ and $\Delta Eswy$ both are negative (northward Bz turning), the slope is higher as compared to the slope when both are positive (southward Bz turning). At first glance it appears that the higher efficiency during northward turning is ambiguous. Because during southward Bz the solar wind-magnetosphere coupling is stronger than that during northward Bz, it should result in higher efficiency during southward Bz.

[34] So in order to understand the observed discrepancy, imagine that Bz acts as a switch: when it is negative (southward), it transfers solar wind energy to the magnetosphere through reconnection, and when it becomes zero, energy transfer through reconnection ceases. When Bz is positive (northward), almost no energy or a small amount of energy can enter into the magnetosphere through reconnection occurring at high latitudes. So one can postulate that during southward Bz turnings, increasing amplitude of southward Bz should enhance the convection and during northward turning decreasing amplitude of southward Bz should cause weakening of convection. The linear relationship has been further analyzed by investigating the effect of actual Bz values (Bz_{int} or Bz_{fin}) by splitting Eswy into positive and negative values instead of net change in Eswy ($\Delta Eswy$). It is evident from Figures 11b, 11d, and 11f that during northward turnings $\Delta EEJ_{Correct}$ has strong correlation with $Eswy_{int}$ as compared to the $Eswy_{fin}$, whereas Figures 11c and 11e indicate that $\Delta EEJ_{Correct}$ has better correlation with $Eswy_{fin}$ during southward turnings. Also, during southward turning, the strong correlation of ΔPCN, ΔAL, and ΔAU with $Eswy_{fin}$ as compared to $Eswy_{int}$ supports the above discussed Bz orientation effect on magnetosphere-ionosphere coupling. This clearly shows that during northward turnings, the decrease in southward Bz value mainly contributes to the observed decrease in PPE amplitude in EEJ. Thus, the enhanced magnetospheric reconnection leading to stronger magnetospheric convection during increasing southward Bz and ceasing of convection occurring due to decreasing southward Bz amplitude during northward Bz turning can be ascribed to the observed linearity between ΔEEJ and $\Delta Eswy$. This is a very important observation which may indicate that only southward Bz has major contribution in the observed effect at the equator. During the northward turning, the effect is seen only due to the decreasing values of southward Bz. Even after considering actual Bz values, we observe the higher slope of $Eswy_{int}$ versus $\Delta EEJ_{Correct}$ for northward turning (Figure 11d) as compared to the slope of $Eswy_{fin}$ versus $\Delta EEJ_{Correct}$ for southward turning (Figure 11e) indicating higher efficiency of PPE during northward as compared to southward turnings. This should be due to the fact that overshielding effect due to Region-2 field-aligned currents are also contributing during northward turnings in addition to the effect of the decreasing convection, whereas during southward turnings only the effect of increasing convection is contributing to the increase of the amplitude of PPE signature, hence enhancing the efficiency during northward turnings. Hence, observed differences in the efficiency during southward and northward turnings can be attributed to the presence of dusk-to-dawn shielding electric field in the inner magnetosphere, thus emphasizing the role of over-shielding during northward Bz.

[35] **Acknowledgments.** The solar wind parameters, interplanetary magnetic field, and geomagnetic indices used in this paper are obtained form CDAWEB. PCN index is made available by Danish Meteorological Institute, Copenhagen, Denmark. We thank ACE Science Center and Danish Meteorological Institute for providing data. Authors thank observatory and data processing staff of Indian Institute of Geomagnetism. Authors would also like to thank R. Rajaram for valuable discussions.

[36] Robert Lysak thanks the reviewers for their assistance in evaluating this paper.

References

Abdu, M. A., T. Maruyama, I. S. Batista, S. Saito, and M. Nakamura (2007), Ionospheric responses to the October 2003 superstorm: Longitude/local time effects over equatorial low and middle latitudes, *J. Geophys. Res.*, *112*, A10306, doi:10.1029/2006JA012228.

Anderson, D., A. Anghel, K. Yumoto, M. Ishitsuka, and E. Kudeki (2002), Estimating daytime vertical $E \times B$ drift velocities in the equatorial *F*-region using ground-based magnetometer observations, *Geophys. Res. Lett.*, *29*, 1596, doi:10.1029/2001GL014562.

Bak, P., C. Tang, and K. Wiesenfeld (1987), Self-organized criticality: An explanation of the 1/*f* noise, *Phys. Rev. Lett.*, *59*, 381–384.

Blanc, M., and A. D. Richmond (1980), The ionospheric disturbance dynamo, *J. Geophys. Res.*, *85*, 1669–1686.

Clauer, C. R., and E. Friis-Christensen (1988), High-latitude dayside electric fields and currents during strong northward interplanetary magnetic field: Observations and model simulation, *J. Geophys. Res.*, *93*, 2749–2757.

Cumnock, J. A., R. A. Heelis, M. R. Hairston, and P. T. Newell (1995), High-latitude ionospheric convection pattern during steady northward interplanetary magnetic field, *J. Geophys. Res.*, *100*, 14,537–14,555.

Dungey, J. W. (1961), Interplanetary magnetic field and the auroral zones, *Phys. Rev. Lett.*, *6*, 47–48.

Etemadi, A., S. W. H. Cowley, M. Lockwood, B. J. L. Bromage, and D. M. Willis (1988), The dependence of high-latitude dayside ionospheric flows on the north-south component of the IMF: A high time resolution correlation analysis using EISCAT "POLAR" and AMPTE UKS and IRM data, *Planet. Space Sci.*, *36*, 471–498.

Fejer, B. G., C. A. Gonzales, D. T. Farley, M. C. Kelley, and R. F. Woodman (1979), Equatorial electric fields during magnetically disturbed conditions 1. The effect of the interplanetary magnetic field, *J. Geophys. Res.*, *84*, 5797–5802.

Fejer, B. G., J. W. Jensen, T. Kikuchi, M. A. Abdu, and J. L. Chau (2007), Equatorial ionospheric electric fields during the November 2004 magnetic storm, *J. Geophys. Res.*, *112*, A10304, doi:10.1029/2007JA012376.

Gonzalez, W. D., E. Echer, B. T. Tsurutani, A. L. Clúa de Gonzalez, and A. Dal Lago (2011), Interplanetary origin of intense, superintense and extreme geomagnetic storms, *Space Sci. Rev.*, *158*, 69–89.

Guo, J., X. Feng, P. Zuo, J. Zhang, Y. Wei, and Q. Zong (2011), Interplanetary drivers of ionospheric prompt penetration electric fields, *J. Atmos. Sol. Terr. Phys.*, *73*, 130–136.

Huang, C., G. J. Sofko, A. V. Koustov, and D. A. Andre (2000), Evolution of ionospheric multicell convection during northward interplanetary magnetic field with $|Bz/By| > 1$, *J. Geophys. Res.*, *105*, 27,095–27,107.

Huang, C., J. C. Foster, and M. C. Kelley (2005), Long-duration penetration of the interplanetary electric field to the low-latitude ionosphere during the main phase of magnetic storms, *J. Geophys. Res.*, *110*, A11309, doi:10.1029/2005JA011202.

Huang, C., I. Sazykin, R. Spiro, J. Goldstein, G. Crowley, and J. M. Ruohoniemi (2006), Storm-time penetration electric fields and their effects, *Eos Trans. AGU*, *87*(13), 131.

Huang, C., S. Sazykin, J. L. Chau, N. Maruyama, and M. C. Kelley (2007), Penetration electric fields: Efficiency and characteristic time scale, *J. Atmos. Sol. Terr. Phys.*, *69*, 1135–1146.

Iijima, T. (1984), Field-aligned currents during northward IMF, in *Magnetospheric Currents, Geophys. Monogr. Ser.,* vol. 28, edited by T. A. Potemra, pp. 115–122, AGU, Washington, D. C., doi:10.1029/GM028p0115.

Kelley, M. C., B. G. Fejer, and C. A. Gonzales (1979), An explanation for anomalous equatorial ionospheric electric fields associated with a northward turning of the interplanetary magnetic field, *Geophys. Res. Lett.*, *6*, 301–304.

Kelley, M. C., J. J. Makela, J. L. Chau, and M. J. Nicolls (2003), Penetration of the solar wind electric field into the magnetosphere/ionosphere system, *Geophys. Res. Lett.*, *30*(4), 1158, doi:10.1029/2002GL016321.

Kikuchi, T., T Araki, H. Maeda, and K. Maekawa (1978), Transmission of polar electric fields to the equator, *Nature*, *273*, 650–651.

Kikuchi, T., and T. Araki (1979), Horizontal transmission of the polar electric field to the equator, *J. Atmos. Terr. Phys.*, *41*, 927–936.

Kikuchi, T., H. Lühr, T. Kitamura, O. Saka, and K. Schlegel (1996), Direct penetration of the polar electric field to the equator during a *DP* 2 event as detected by the auroral and equatorial magnetometer chains and the EISCAT radar, *J. Geophys. Res.*, *101*, 17,161–17,173.

Kikuchi, T., H. Lühr, K. Schlegel, H. Tachihara, M. Shinohara, and T.-I. Kitamura (2000), Penetration of auroral electric fields to the equator during a substorm, *J. Geophys. Res.*, *105*, 23,251–23,261.

Kikuchi, T., Y. Ebihara, K. K. Hashimoto, R. Kataoka, T. Hori, S. Watari, and N. Nishitani (2010), Penetration of the convection and overshielding electric fields to the equatorial ionosphere during a quasiperiodic *DP* 2 geomagnetic fluctuation event, *J. Geophys. Res.*, *115*, A05209, doi:10.1029/2008JA013948.

Khan, H., and S. W. H. Cowley (1999), Observations of the response time of high-latitude ionospheric convection to variations in the interplanetary magnetic field using EISCAT and IMP-8 data, *Ann. Geophys.*, *17*, 1306–1335.

Knipp, D. J., et al. (1993), Ionospheric convection response to slow, strong variations in a northward interplanetary magnetic field: A case study for January 14, 1988, *J. Geophys. Res.*, *98*, 19,273–19,292.

Lockwood, M., A. P. van Eyken, B. J. I. Bromage, and D. M. Willis (1986), Eastward propagation of a plasma convection enhancement following a southward turning of the interplanetary magnetic field, *Geophys. Res. Lett.*, *13*, 72–75.

Lu, E. T., and R. J. Hamilton (1991), Avalanches and the distribution of solar flares, *Astrophys. J.*, *380*, L89–L92.

Manoj, C., S. Maus, H. Luhr, and P. Alken (2008), Penetration characteristics of the interplanetary electric field to the daytime equatorial ionosphere, *J. Geophys. Res.*, *113*, A12310, doi:10.1029/2008JA013381.

Murr, D. L., and W. J. Hughes (2001), Reconfiguration timescales of ionospheric convection, *Geophys. Res. Lett.*, *28*, 2145–2148.

Nishida, A., N. Iwasaki, and T. Nagata (1966), The origin of fluctuations in the equatorial electrojet: A new type of geomagnetic variation, *Ann. Geophys.*, *22*, 478–484.

Nishida, A. (1968), Coherence of geomagnetic *DP* 2 fluctuations with interplanetary magnetic variations, *J. Geophys. Res.*, *73*, 5549–5559.

Onwumechilli, A., and P. O. Ogbuehi (1962), Fluctuations in the geomagnetic horizontal field, *J. Atmos. Terr. Phys.*, *24*, 173–190.

Patel, V. L. (1978), Interplanetary magnetic field variations and the electromagnetic state of the equatorial ionosphere, *J. Geophys. Res.*, *83*, 2137–2144.

Rastogi, R. G., and V. L. Patel (1975), Effect of interplanetary magnetic field on ionosphere over the magnetic equator, *Proc. Indian Natl. Sci. Acad.*, *82*, 121–141.

Rastogi, R. G., and J. A. Klobuchar (1990), Ionospheric electron content within the equatorial F_2 layer anomaly belt, *J. Geophys. Res.*, *95*, 19,045–19,052.

Ridley, A. J., G. Lu, C. R. Clauer, and V. O. Papitashvili (1998), A statistical study of the ionospheric convection response to changing interplanetary magnetic field conditions using the assimilative mapping of ionospheric electrodynamics technique, *J. Geophys. Res.*, *103*, 4023–4039.

Ruohoniemi, J. M., and R. A. Greenwald (1998), The response of high-latitude convection to a sudden southward IMF turning, *Geophys. Res. Lett.*, *25*, 2913–2916.

Scott, D. W. (1979), On optimal and data-based histograms, *Biometrika*, *66*, 605–610.

Simi, K. G., S. V. Thampi, D. Chakrabarty, B. M. Pathan, S. R. Prabhakaran Nayar, and T. K. Pant (2012), Extreme changes in the equatorial electrojet under the influence of interplanetary electric field and the associated modification in the low-latitude *F* region plasma distribution, *J. Geophys. Res.*, *117*, A03331, doi:10.1029/2011JA017328.

Todd, H., S. W. H. Cowely, M. Lockwood, and D. M. Willis (1988), Response time of the high-latitude dayside ionosphere to sudden changes in the north-south component of the IMF, *Planet. Space Sci.*, *36*, 1415–1428.

Troshichev, O. A., and V. G. Andrezen (1985), The relationship between interplanetary quantities and magnetic activity in the southern polar cap, *Planet. Space Sci.*, *33*, 415–419.

Troshichev, O. A., V. G. Andrezen, S. Vennerstroem, and E. Friis-Christensen (1988), Magnetic activity in the polar cap—A new index, *Planet. Space Sci.*, *36*, 1095–1102.

Troshichev, O., A. Janzhura, and P. Stauning (2006), Unified PCN and PCS indices: Method of calculation, physical sense, and dependence on the IMF azimuthal and northward components, *J. Geophys. Res.*, *111*, A05208, doi:10.1029/2005JA011402.

Tsuji, Y., A. Shinbori, T. Kikuchi, and T. Nagatsuma (2012), Magnetic latitude and local time distributions of ionospheric currents during a geomagnetic storm, *J. Geophys. Res.*, *117*, A07318, doi:10.1029/2012JA017566.

Wei, Y., W. Wan, Z. Pu, M. Hong, Q. Zong, J. Guo, B. Zhao, and Z. Ren (2011), The transition to overshielding after sharp and gradual interplanetary magnetic field northward turning, *J. Geophys. Res.*, *116*, A01211, doi:10.1029/2010JA015985.

Weimer, D. R. (1995), Models of high-latitude electric potentials derived with a least error fit of spherical harmonic coefficients, *J. Geophys. Res.*, *100*, 19,595–19,607.

Wolf, R. A., R. W. Spiro, S. Sazykin, and F. R. Toffoletto (2007), How the Earth's inner magnetosphere works: An evolving picture, *J. Atmos. Sol. Terr. Phys.*, *69*, 288–302.